Transverse dielectric matrix and shear mode dispersion in strongly coupled electronic bilayer liquids

Kenneth I Golden* and Hania Mahassen
Department of Mathematics and Statistics, College of Engineering and Mathematical Sciences, University of Vermont, Burlington, Vermont 05401-1455, USA

Gaetano Senatore†
Dipartimento di Fisica Teorica, Università di Trieste, Strada Costiera 11, 34014 Trieste, Italy and INFM-CNR-Democritos National Simulation Center, Trieste, Italy

Francesco Rapisarda‡
Dipartimento di Fisica Teorica, Università di Trieste, Strada Costiera 11, 34014, Trieste, Italy

(Received 23 August 2006; revised manuscript received 18 September 2006; published 29 November 2006)

The authors develop a transverse dielectric matrix and from it they calculate the shear mode dispersion in strongly coupled charged-particle bilayer liquids in the $T=0$ quantum domain. The formulation is based on the classical quasilocalized charge approximation (QLCA) and extends the QLCA formalism into the quantum domain. Its development parallels and complements the development of a similarly extended longitudinal dielectric matrix formalism reported in a recent companion work [K. I. Golden, H. Mahassen, G. J. Kalman, G. Senatore, and F. Rapisarda, Phys. Rev. E **71**, 036401 (2005)]. Using pair correlation function data generated from diffusion Monte Carlo simulations, the authors calculate the dispersion of the in-phase and out-of-phase shear modes over a wide range of high-r_s values and layer separations. Over the coupling range $10 \leq r_s \leq 30$ and for layer separations $0.2/\sqrt{\pi n} \leq d \leq 0.5/\sqrt{\pi n}$, the present study predicts the existence of a robust out-of-phase gapped shear mode dispersion in the domain of the q,ω-plane above the left boundary of the RPA single-pair excitation region; under these conditions, the out-of-phase collective excitation is entirely immune to Landau damping and can be safely considered to be mostly unaffected by diffusive-migrational damping.

DOI: 10.1103/PhysRevE.74.056405 PACS number(s): 52.27.Gr, 52.25.Mq, 73.21.−b, 73.20.Mf

I. INTRODUCTION

By now, it is well documented that Coulomb [1–10] and complex plasma [11–17] systems in the strongly correlated liquid phase can support transverse shear waves. This is borne out by molecular dynamics (MD) simulations [1,2,6,10,11,13] performed on a variety of classical charged-particle liquid-phase configurations over the past three decades, beginning with the classical three-dimensional (3D) one-component plasma (OCP) [1,6] and progressing to more recent MD simulations of electronic bilayer liquids [10] and complex plasmas [11,13]. Recent experiments carried out by Piel, Nosenko and Goree [17] confirm the existence of strongly to moderately damped shear waves in 2D complex (dusty) plasmas in the strongly coupled liquid phase.

Numerous theoretical studies of transverse shear mode dispersion in classical charged-particle liquids have been carried out. Agarwal, Thakur and Pathak [3] derived the second frequency-moment sum rule for the transverse current correlation function in 2D classical electron liquids and used the sum rule to infer the shear mode oscillation frequency. The quasilocalized charge approximation (QLCA) formulated by Kalman and Golden [9,16] has been repeatedly used to calculate transverse shear mode dispersion in the 3D classical OCP [4], in layered classical electron liquids [5,7–10], and in 3D and 2D Yukawa liquids [12,13]. Shear mode dispersion relations for 3D Yukawa liquids have also been derived by Kaw and Sen [14] using a generalized hydrodynamics description of the dust dynamics, and by Murillo [15] using a Mori memory function approach based on the generalized viscosity.

To date, all of the above investigations have been carried out in the classical domain, and, to the best of our knowledge, the problem of transverse shear mode dispersion in Coulomb liquids in the quantum domain remains largely unexplored. Of particular interest in this regard are semiconductor layered electron (hole) liquids in the low-density (high-r_s) regime. In the area of condensed matter plasmas, there has been considerable interest in fabricating such charged-particle systems. So far, advances in modern semiconductor technology have made it possible to routinely fabricate high mobility single 2D layers in a strongly correlated Coulomb liquid at temperatures well below and comparable with the Fermi temperature [18]. Experimental studies carried out in this domain include recent inelastic light-scattering based measurements of longitudinal plasmon dispersion in high-quality, low-density 2D electron liquids [19]. One would expect that similar high-r_s experimental techniques—applied as well to measurements of shear mode dispersion—will become available also to bilayers and double quantum wells in the near future. In this context, the theoretical study proposed in the present work would seem to be especially timely.

*Also at Department of Physics, University of Vermont, Burlington, VT 05405, USA.
†Electronic address: senatore@ts.infn.it
‡Present Address: USB Investment Bank, London, England.

This paper addresses the problem of transverse shear mode dispersion in strongly coupled electronic bilayer liquids in the zero-temperature ($T=0$) quantum domain. The symmetric bilayer is modeled as two equal-density ($n_1=n_2=n=N/\Omega$) monolayers of mobile electrons (or holes), each layer immersed in its own 2D uniform neutralizing background of opposite charge. The N charges in each monolayer occupy the large but bounded area Ω in the planes $z=0$ and $z=d$ of a Cartesian coordinate system. In the present study, the interlayer spacing d always exceeds the effective Bohr radius, $a_B=\hbar^2\varepsilon_s/me^2$ (ε_s is the dielectric constant of the substrate), so that interlayer tunneling can be neglected. The interaction potentials for the symmetric charged-particle bilayer are given as

$$\phi_{11}(r)=\phi_{22}(r)=e^2/(\varepsilon_s r), \quad \phi_{12}(r)=e^2/(\varepsilon_s\sqrt{r^2+d^2}),$$

$$\phi_{11}(q)=\phi_{22}(q)=2\pi e^2/(\varepsilon_s q),$$

$$\phi_{12}(q)=[2\pi e^2/(\varepsilon_s q)]\exp(-qd), \tag{1}$$

r and q being the in-layer separation distance and wave number, respectively. The parameter $r_s=a/a_B$ is the customary measure of the in-layer coupling strength in the zero-temperature quantum domain; $a=1/\sqrt{\pi n}$ is the 2D Wigner-Seitz radius.

The approach followed in this paper is based on an extension of the transverse QLCA into the quantum domain. The QLCA has proved to be consistently successful in the description of collective mode dispersion in classical Coulomb liquids as borne out by comparisons with a series of MD simulations [2,6,9,10,13]. In the QLCA description of strongly coupled Coulomb liquids, the charged particles are trapped in local potential fluctuations. The fluctuating potential creates local momentary potential wells at random locations whose relative positions are strongly correlated with each other. Particles oscillate in the potential wells while the potential landscape dissolves into a different structure on a longer time scale. As a result, the particles slowly diffuse out from their temporary locations, leading to damping of the oscillations. Self diffusion is the principal transport mechanism underlying this damping [4,5,8,9]. A first-principles microscopic procedure has yet to be worked out for incorporating this "diffusive-migrational" damping mechanism into the QLCA formalism. So, as in all the previous QLCA studies of collective mode dispersion in classical Coulomb and Yukawa liquids, its incorporation in the collective mode analysis of the present work will be done on an *ad hoc* basis.

The development to be followed here parallels that of a recent companion paper [20] (see also Ref. [21]) in which the longitudinal QLCA dielectric matrix was extended in a way that made it suitable for the description of plasmon dispersion in strongly coupled electronic bilayers in the zero-temperature quantum domain.

According to the QLCA description of the classical bilayer liquid [8–10], the transverse shear mode structure consists of an acoustic ($\omega \propto q$) in phase (+) mode (where the two layers oscillate in unison) and a gapped out-of-phase (–) mode (where the oscillations of the two layers exhibit a 180° phase difference). The out-of-phase transverse shear and longitudinal plasma modes share the same $q=0$ finite frequency energy gap [10].

Crucial to the extended QLCA approach is the description of the positions of the localized particles in terms of equilibrium pair distribution functions. The latter, along with the phase diagram for the symmetric electronic bilayer liquid, has been generated over a wide range of r_s and d/a values from diffusion Monte Carlo (DMC) simulations carried out by Rapisarda and Senatore [20,22(a)–22(d),22(f)]. A full compilation of the details of their DMC study is also available [22(e)].

Both the DMC simulations and the extended quantum QLCA calculations in the present work are limited to the extent that tunneling between the two layers is ignored. Consequently, the range of validity for the present analysis is necessarily restricted to layer separations $d>a_B$. Note, however, that for $r_s>1$, this condition still substantially allows for $d<a$, and, consequently, for *strong* interlayer interactions.

The organization of the paper is as follows. In Sec. II, we develop the extended transverse QLCA for charged-particle bilayer liquids and we formulate the transverse dielectric matrix $\varepsilon_{AB}^T(\mathbf{q},\omega)$ and its in-phase (+) and out-of-phase (–) matrix elements $\varepsilon_{\pm}^T(\mathbf{q},\omega)$. The transverse dielectric matrix elements go beyond the RPA in that they contain static in-layer exchange-correlation and interlayer correlation contributions $G_{AB}^T(\mathbf{q})$ that are ultimately expressed in terms of the pair correlation functions generated from the DMC computer simulations [20] cited above. Formulas expressing $G_{AB}^T(q\rightarrow 0)$ in terms of inlayer and interlayer interaction energies are displayed in Sec. II. In Sec. III, we analyze the transverse shear mode relations in the non-retarded (quasistatic) limit that result from the zeros of $1/\varepsilon_{\pm}^T(q,\omega)$. Conclusions are drawn in Sec. IV.

A main ingredient of the Sec. II formulation of the transverse dielectric matrix is the 2D current-density transverse Lindhard function $\chi_0^T(\mathbf{q},\omega)$. A variant of it was derived some time ago by Toyoda, Gudmundsson, and Takahashi [23(a)]; see also Ref. [23(b)]. In the Appendix, we derive the 2D Lindhard formula for $\chi_0^T(\mathbf{q},\omega)$ in a form that is especially well tailored to its implementation in the QLCA formalism of the present work. The Appendix derivation parallels the Ehrenreich-Cohen [24] and Kliewer-Fuchs [25] self-consistent field (SCF) calculations for the three-dimensional electron gas.

II. TRANSVERSE DIELECTRIC MATRIX

In this section, we formulate the transverse dielectric response matrix for strongly coupled charged-particle bilayer liquids in the zero-temperature quantum domain. Parallel to the development Ref. [20], the starting point for the present derivation is the classical (cl) layer-space dielectric matrix, $\varepsilon_{AB}^T(\mathbf{q},\omega)$, that results from the QLCA [9]:

$$\varepsilon_{AB}^{T}(\mathbf{q},\omega)\big|_{cl} = \delta_{AB} - \frac{q^2c^2}{\omega^2}\sum_{C}\psi_{AC}(q,\omega) \times \frac{n}{mc^2}\left[\underset{\approx}{\mathbf{I}} - \frac{q^2c^2}{\omega^2}\frac{n}{mc^2}\underset{\approx}{\mathbf{D}}^{T}(\mathbf{q})\right]^{-1}_{CB}, \tag{2}$$

A, B, C indices label the layers ($A,B,C=1,2$); the T superscript indicates transverse (with respect to in-plane wave vector $\mathbf{q}$) elements of the dielectric tensor $\underset{\approx}{\epsilon}_{AB}$; $\psi_{AB}(q,\omega) = \phi_{AB}(q)[\beta(q,\omega)/q]$ is the layer-layer interaction potential matrix featuring the familiar attenuation constant $\beta(q,\omega) = \sqrt{q^2-\omega^2/c^2}$ that shows up in the phenomenological electrodynamics of 2D [26] and layered charged-particle structures [27]; $\underset{\approx}{\mathbf{I}}$ is the (2×2) identity matrix and $(nq^2/m)\underset{\approx}{\mathbf{D}}^{T}(\mathbf{q})$ is the non-RPA correlational part of the transverse dynamical matrix. Equation (2) is derived from the microscopic equation of motion for the collective coordinates $\vec{\xi}_A^{\mathbf{q}}(t)$, defined through the Fourier representation $\vec{\xi}_A^{i}(t) = (1/\sqrt{Nm})\Sigma_{\mathbf{q}}\vec{\xi}_A^{q}(t)\exp(i\mathbf{q}\cdot\mathbf{x}_A^i)$ relating $\vec{\xi}_A^{\mathbf{q}}$ to the displacement $\vec{\xi}_A^{i}$ of particle i in layer A. The QLCA matrix elements are expressed in terms of $S_{11}(\mathbf{q})$, $S_{12}(\mathbf{q})$ structure factors, or equivalently, in terms of the corresponding equilibrium pair correlation functions $h_{AB}(r)=(1/N)\Sigma_{\mathbf{q}}[S_{AB}(\mathbf{q}) - \delta_{AB}]\exp(i\mathbf{q}\cdot\mathbf{r})$ [8,9]:

$$D_{11}^{T}(\mathbf{q}) = \frac{1}{N}\sum_{\mathbf{q}'}\left[\frac{q'^2}{q^2} - \frac{(\mathbf{q}\cdot\mathbf{q}')^2}{q^4}\right]\phi_{11}(q')[S_{11}(|\mathbf{q}-\mathbf{q}'|) - S_{11}(q')] - \frac{1}{N}\sum_{\mathbf{q}'}\left[\frac{q'^2}{q^2} - \frac{(\mathbf{q}\cdot\mathbf{q}')^2}{q^4}\right]\phi_{12}(q')S_{12}(q') \tag{3a}$$

$$= \frac{\pi e^2}{q^2}\int_0^\infty dr\frac{1}{r^2}h_{11}(r)\left[1 + 2J_0(qr) - 6\frac{J_1(qr)}{qr}\right] + \frac{\pi e^2}{q^2}\int_0^\infty dr\frac{rh_{12}(r)}{(r^2+d^2)^{3/2}}\left[1 - \frac{3d^2}{r^2+d^2}\right], \tag{3b}$$

$$D_{12}^{T}(\mathbf{q}) = \frac{1}{N}\sum_{\mathbf{q}'}\left[\frac{q'^2}{q^2} - \frac{(\mathbf{q}\cdot\mathbf{q}')^2}{q^4}\right]\phi_{12}(q')S_{12}(|\mathbf{q}-\mathbf{q}'|) \tag{4a}$$

$$= -\frac{\pi e^2}{q^2}\int_0^\infty dr\frac{rh_{12}(r)}{(r^2+d^2)^{3/2}}\left[1 - \frac{3d^2}{r^2+d^2}\right] + \frac{\pi e^2}{q^2}\int_0^\infty dr\frac{rh_{12}(r)}{(r^2+d^2)^{3/2}} \times \left[1 + 2J_0(qr) - 6\frac{J_1(qr)}{qr}\right] - \frac{3\pi e^2 d^2}{q^2} \times \int_0^\infty dr\frac{rh_{12}(r)}{(r^2+d^2)^{5/2}}\left[1 - 2\frac{J_1(qr)}{qr}\right], \tag{4b}$$

$J_0(qr)$ and $J_1(qr)$ are Bessel functions of order zero and one, respectively. At long wavelengths ($q\to 0$), Eqs. (3a) and (4a) simplify to

$$D_{11}^{T}(q\to 0) = -\frac{1}{16N}\sum_{\mathbf{q}'}\phi_{11}(q')[S_{11}(q')-1] - \frac{1}{2Nq^2}\sum_{\mathbf{q}'}q'^2\phi_{12}(q')S_{12}(q'), \tag{5}$$

$$D_{12}^{T}(q\to 0) = \frac{1}{2Nq^2}\sum_{\mathbf{q}'}q'^2\phi_{12}(q')S_{12}(q') - \frac{1}{16N}\sum_{\mathbf{q}'}\phi_{12}(q')S_{12}(q')[1 + q'd - q'^2d^2]. \tag{6}$$

The expressions (3) and (4) can be readily identified as the correlational contributions to the non-retarded second-frequency-moment sum rules

$$\langle\omega_{AB}^2\rangle(\mathbf{q}) = \beta m\int_{-\infty}^{\infty}\frac{d\omega}{2\pi}\omega^2 C_{AB}(\mathbf{q},\omega) = \frac{q^2}{\beta m}\delta_{AB} + \frac{nq^2}{m\Omega}D_{AB}^{T}(\mathbf{q}) \tag{7}$$

for the transverse current-current correlation function

$$C_{AB}(\mathbf{q},t) = \frac{1}{N}\langle j_{\mathbf{q}A}^{T}(t)j_{-\mathbf{q}B}^{T}(0)\rangle; \tag{8}$$

$j_{qA}^{T}(t)=\Sigma_i v_{iA}^{T}(t)exp[-i\mathbf{q}\cdot\mathbf{x}_{iA}]$ is the transverse microscopic particle current density in layer A and $\beta^{-1}=kT$. The assured strict compliance with these sum rules is a crucial ingredient of the QLCA description of electronic bilayer liquids in view of the fact that

$$\langle\omega_{11}^2\rangle(q=0) - \langle\omega_{12}^2\rangle(q=0) = -\frac{1}{m\Omega^2}\sum_{\mathbf{q}'}q'^2\phi_{12}(q')S_{12}(q'), \tag{9}$$

establishes the one-to-one correspondence between the sum rule and the existence of the long-wavelength finite frequency (energy gap [Eq. (25)] below) shared by the out-of-phase plasmon and shear modes. The non-retarded transverse bilayer sum rule formula (7)—reported here for the first time—generalizes the transverse second-frequency-moment sum rule established by Agarwal, Thakur, and Pathak [3] for the isolated 2D classical electron liquid.

Recalling what was stated in Ref. [20], the derivation of Eq. (2) is predicated on the assumption that random motions are negligible: this is a reasonable assumption for a low-temperature classical charged-particle bilayer in the strong coupling regime where the potential energy dominates over the thermal energy that is responsible for random motion, so that at sufficiently low temperatures one can neglect the random motion of the particles. In contrast, for the zero-temperature quantum bilayer, the low temperature does not ensure that the random motion of the particles is negligible, and one should therefore take account of the ground-state kinetic energy of the particles. In order to accomplish this,

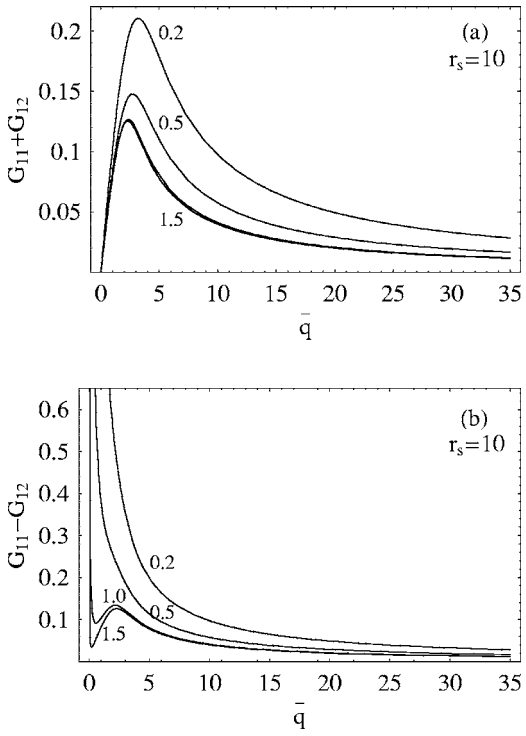

FIG. 1. $G_{11}(\mathbf{q})\pm G_{12}(\mathbf{q})$ as a function of $\bar{q}=q/q_F$ for $r_s=10$ and $d/a=0.2$ (normal fluid), 0.5 (normal fluid), 1.0 (normal fluid), and 1.5 (normal fluid); $q_F=\sqrt{2\pi n}$. The curves are generated from Eqs. (3b) and (4b), and $G_{AB}(\mathbf{q})=[\epsilon_s q(2\pi e^2)D_{AB}^T(\mathbf{q})]$, with the input of diffusion Monte Carlo pair distribution function data [20,22].

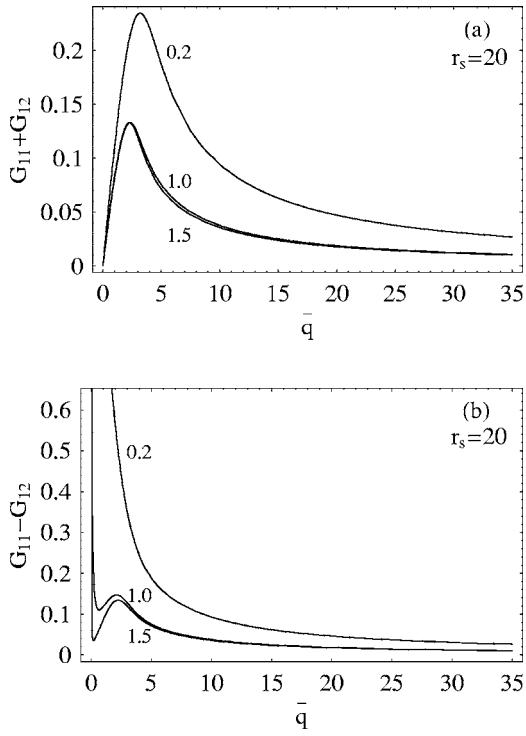

FIG. 2. $G_{11}(\mathbf{q})\pm G_{12}(\mathbf{q})$ as a function of $\bar{q}=q/q_F$ for $r_s=20$ and $d/a=0.2$ (normal fluid), 1.0 (normal fluid), and 1.5 (fully spin-polarized fluid). The curves are generated from Eqs. (3b) and (4b), and $G_{AB}(\mathbf{q})=[\epsilon_s q/(2\pi e^2)D_{AB}^T(\mathbf{q})]$, with the input of diffusion Monte Carlo pair distribution function data [20,22].

we observe that, in Eq. (2), the $-n/mc^2$ factor can be immediately identified as the Vlasov value of the 2D current-density response function [compare Eqs. (2) and (A22)] corresponding to the kinetic momentum distribution function $f(\mathbf{p})\approx n\delta(\mathbf{p})$. One may therefore assume that for a Fermi distribution of momenta, the appropriate replacement for $-n/mc^2$ is the Lindhard current-density response matrix $\chi_{AB}^{T(0)}(\mathbf{q},\omega)=\chi_0^T(\mathbf{q},\omega)\delta_{AB}$, where (see the Appendix)

$$\chi_0^T(\mathbf{q},\omega)=-\frac{n}{mc^2}\left\{1+\frac{2\hbar^2}{Nm}\sum_{\mathbf{k}}\left[k^2-\frac{(\mathbf{k}\cdot\mathbf{q})^2}{q^2}\right]\times\frac{f(\varepsilon_{\mathbf{k}+\mathbf{q}})-f(\varepsilon_{\mathbf{k}})}{\varepsilon_{\mathbf{k}+\mathbf{q}}-\varepsilon_{\mathbf{k}}+\hbar\,\omega+io}\right\}, \tag{10}$$

$f(\varepsilon_{\mathbf{k}})$ is the equilibrium Fermi function for a free electron with energy $\epsilon_{\mathbf{k}}=\hbar^2k^2/2m$. The resulting dielectric matrix takes the form

$$\varepsilon_{AB}^T(\mathbf{q},\omega)=\delta_{AB}+\frac{q^2c^2}{\omega^2}\sum_C\psi_{AC}(q,\omega)\chi_0^T(\mathbf{q},\omega)\times\left[\underset{\approx}{\mathbf{I}}+\frac{q^2c^2}{\omega^2}\chi_0^T(\mathbf{q},\omega)\underset{\approx}{\mathbf{D}}^T(\mathbf{q})\right]_{CB}^{-1} \tag{11}$$

$(A,B,C=1,2)$. We note that the transverse dielectric matrix (11) and all other physical quantities can be diagonalized by rotating into the space spanned by the in-phase (+) and out-of-phase (−) directions: for the symmetric bilayer the resulting matrix elements are $\varepsilon_\pm(\mathbf{q},\omega)=\varepsilon_{11}(\mathbf{q},\omega)\pm\varepsilon_{12}(\mathbf{q},\omega)$, $\psi_\pm(q,\omega)=\psi_{11}(q,\omega)\pm\psi_{12}(q,\omega)$, etc. For notational convenience, we introduce the function $\xi_0^T(\mathbf{q},\omega)=(q^2c^2/\omega^2)\chi_0^T(\mathbf{q},\omega)$, which masks the retardation effect, that is,

$$\xi_0^T(\mathbf{q},\omega)=-\frac{nq^2}{m\omega^2}\left\{1+\frac{2\hbar^2}{Nm}\sum_{\mathbf{k}}\left[k^2-\frac{(\mathbf{k}\cdot\mathbf{q})^2}{q^2}\right]\times\frac{f(\varepsilon_{\mathbf{k}+\mathbf{q}})-f(\varepsilon_{\mathbf{k}})}{\varepsilon_{\mathbf{k}+\mathbf{q}}-\varepsilon_{\mathbf{k}}+\hbar\,\omega+io}\right\}. \tag{12}$$

Upon diagonalizing Eq. (11) and then going to the nonretarded $(c\to\infty)$ limit, the limit that is of interest in the present work, we obtain the compact expression

$$\varepsilon_\pm^T(\mathbf{q},\omega)=1+\frac{\phi_\pm(q)\xi_0^T(\mathbf{q},\omega)}{1+\xi_0^T(\mathbf{q},\omega)[D_{11}^T(\mathbf{q})\pm D_{12}^T(\mathbf{q})]}. \tag{13}$$

The $D_{11}^T(\mathbf{q})$ and $D_{12}^T(\mathbf{q})$ matrix elements in Eqs. (11) and (13) are formally identical to $D_{11}^T(\mathbf{q})$ and $D_{12}^T(\mathbf{q})$ in Eqs. (3) and (4), but it should be borne in mind that $S_{AB}(q)$, $h_{AB}(r)$, etc., are now the static structure functions and pair correlation functions appropriate for the electronic bilayer liquid in the zero-temperature quantum domain and, as such, these quantities embody all the exchange-correlation effects. Accordingly, $D_{11}^T(\mathbf{q})$ and $D_{12}^T(\mathbf{q})$ are to be calculated from Eqs. (3b)

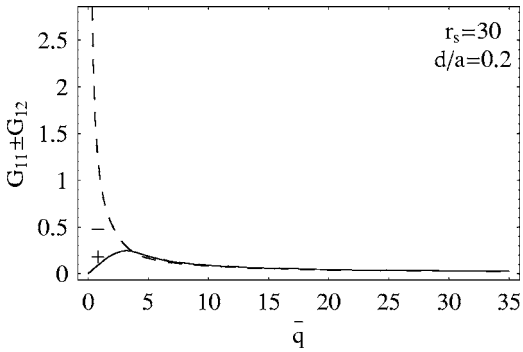

FIG. 3. $G_{11}(\mathbf{q})\pm G_{12}(\mathbf{q})$ as a function of $\bar{q}=q/q_F$ for $r_s=30$ and $d/a=0.2$ (normal fluid). The curves are generated from Eqs. (3b) and (4b), and $G_{AB}(\mathbf{q})=[\epsilon_s q/(2\pi e^2)D^T_{AB}(\mathbf{q})]$, with the input of diffusion Monte Carlo pair distribution function data [20,22].

and (4b) with the input of the diffusion Monte Carlo (DMC) pair distribution function data [20,22(a),22(c),22(f)].

The various relevant phases of the symmetric electronic bilayer at zero temperature have been mapped by Rapisarda and Senatore in Refs. [22(a),22(d)] and are further described in some detail in Ref. [20] along with the DMC pair distribution function data. At $r_s=10,30$, the normal fluid (spin-unpolarized) $g_{AB}(r)=1+h_{AB}(r)$ data displayed in Figs. 1 and 3 of Ref. [20] are the appropriate inputs into the Eqs. (3b) and (4b) for the computation of $D^T_{11}(\mathbf{q})$ and $D^T_{12}(\mathbf{q})$. At $r_s=20$ and $d/a=0.2$, the appropriate inputs again are the normal fluid $g_{AB}(r)$ data displayed in Fig. 2 of Ref. [20]; for $d/a=1.0$ and 1.5, the $g_{AB}(r)$ data for the fully spin-polarized and normal fluids are very nearly the same. Thus, it makes little difference which of these data are selected as inputs into Eqs. (3b) and (4b). We have chosen as inputs the spin-unpolarized data for $r_s=20$, $d/a=1.0$ and the fully spin-polarized data for $r_s=20$, $d/a=1.5$ (also displayed in Fig. 2 of Ref. [20]).

To facilitate the collective mode analysis that follows in Sec. III, we introduce the more convenient dimensionless quantity $G_{AB}(\mathbf{q})=[\epsilon_s q/(2\pi e^2)]D^T_{AB}(\mathbf{q})$, which formally resembles a static local field correction. However, one should bear in mind that, similarly to the Ref. [20] companion longitudinal study, the physical justification for this term is different from that of the conventional static mean field. $G^T_{11}(\mathbf{q})\pm G^T_{12}(\mathbf{q})$ are shown in Figs. 1–3 as functions of dimensionless in-plane wave number $\bar{q}=q/q_F$ for different r_s and d/a values; $q_F=\sqrt{2\pi n}$ is the 2D Fermi wave number. The small-q behavior of G^T_{11} and G^T_{12} is given by Eqs. (5) and (6) which stipulate that to lowest order in q,

$$G_{11}(q\to 0)+G_{12}(q\to 0) = -\frac{\sqrt{2}}{16}\left[\frac{E_{11}+E_{12}}{e^2/a}\right]\bar{q}-\frac{\sqrt{2}\bar{q}}{16(e^2/a)}\frac{n}{\Omega}\times\sum_{\mathbf{q}'}\phi_{12}(q')h_{12}(q')(q'd-2q'^2d^2), \quad (14)$$

$$G_{11}(q\to 0)-G_{12}(q\to 0) = -\frac{1}{q\Omega}\sum_{\mathbf{q}'}q'h_{12}(q')e^{-q'd} = \frac{1}{2q}\int_0^\infty dr\frac{rh_{12}(r)}{(r^2+d^2)^{3/2}}\left[1-\frac{3d^2}{r^2+d^2}\right]; \quad (15)$$

$$E_{11}=(n/2)\int d\mathbf{r}\phi_{11}(r)h_{11}(r)=(1/2\Omega)\sum_{\mathbf{q}}\phi_{11}(q)[S_{11}(q)-1], \quad (16)$$

$$E_{12}=(n/2)\int d\mathbf{r}\phi_{12}(r)h_{12}(r)=(1/2\Omega)\sum_{\mathbf{q}}\phi_{12}(q)S_{12}(q). \quad (17)$$

$E_{11}=e^2\varepsilon_{\rm int}/(2a_B)$ represents the total in-layer interaction energy per particle consisting of the inlayer Hartree-Fock exchange and potential energy contributions $\varepsilon_{\rm int}=\varepsilon_{ex}+\varepsilon_{pot}$

$$\varepsilon_{ex}=-\frac{8\sqrt{2}}{3\pi r_s},\quad \varepsilon_{pot}=\frac{1}{r_s}\frac{\partial}{\partial r_s}(r_s^2\varepsilon_c);\quad \text{(Ryd)}, \quad (18)$$

ε_c is the correlation energy per particle in Rydberg units; E_{12} is the interlayer potential energy per particle. Since E_{11} is the main ingredient of the shear mode acoustic velocity in the isolated $(d/a\to\infty)$ 2D electron layer [see Eqs. (26) and (28) and the text that follows], it is instructive to comment on the effect of degeneracy on E_{11}. Equation (18) shows how the genuine Coulomb correlation effects contribute to E_{11} at zero temperature; as a reminder, the kinetic energy for the interacting system also has a somewhat similar correlational part, $\varepsilon^c_{kin}=-(\partial/\partial r_s)(r_s\varepsilon_c)$. At finite temperatures (lower degeneracies), the Hartree-Fock exchange energy and correlational contribution to the kinetic energy are diminished whereas the correlational contribution to the interaction energy is increased, the latter evidently at the expense of the correlational contribution to ε_{kin}. Both the Hartree-Fock exchange energy and the correlational part of the kinetic energy eventually drop off to zero in the high-temperature classical limit, at which point all the Coulomb correlation effects reside solely in the interaction energy, that is, the interaction energy and the correlation energy become one and the same: $E_{11}=E_c=-1.095e^2/a+0.985$ kT [28]. This brings us to the question: to what extent is the value of E_{11} affected by the degree of degeneracy? To address this question, we consider the isolated 2D electron liquid in the strong coupling regime first at zero temperature. At $r_s=20$, $\varepsilon_{ex}=-0.06$ Ryd and using the fitted correlation energy formula (14) of Ref. [29], we calculate $\varepsilon_{pot}=-0.041$ Ryd. These total to $E_{11}=-1.012e^2/a$. Compare this with the $E_{11}=-1.07e^2/a$ value calculated from Lado's fitting formula quoted above for a classical 2D electron liquid at $\Gamma=40$ (keeping in mind the $\Gamma\Leftrightarrow 2r_s$ correspondence) and we arrive at a difference of about 6% between the ground-state and classical interaction energies.

As to the asymptotic behavior of $G_{11}(\mathbf{q})\pm G_{12}(\mathbf{q})$, our analysis indicates that $G_{11}(q\to\infty)\pm G_{12}(q\to\infty)=C_\pm(d/a,r_s)/\bar{q}$; the dependence of the positive constant $C_\pm$

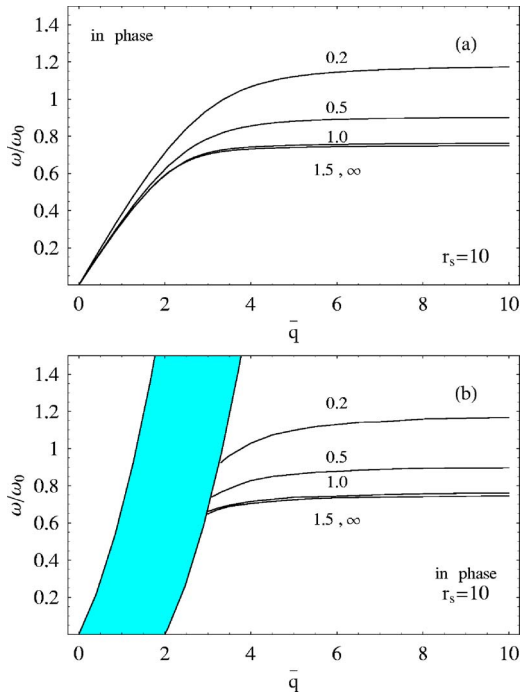

FIG. 4. (Color online) In-phase shear mode dispersion curves for $r_s=10$ and $d/a=0.2$, 0.5, 1.0, 1.5, and ∞. (a) Calculated from primitive transverse QLCA dispersion relation (24) with Eqs. (3b) and (4b). (b) Calculated from extended transverse qQLCA dispersion relation (23) with Eqs. (3b), (4b), (19), and (20). The shaded region in (b) is the RPA pair excitation continuum; $\omega_0=\sqrt{2\pi ne^2/ma}$; $a=1/\sqrt{\pi n}$.

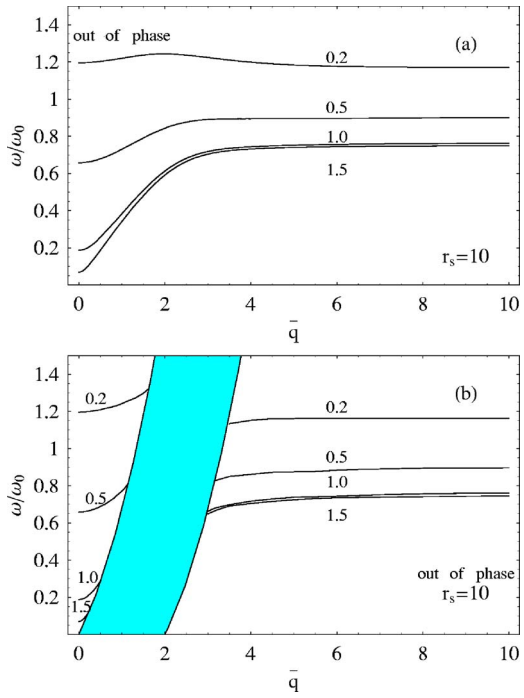

FIG. 5. (Color online) Out-of-phase shear mode dispersion curves for $r_s=10$ and $d/a=0.2$, 0.5, 1.0, and 1.5. (a) Calculated from primitive transverse QLCA dispersion relation (24) with Eqs. (3b) and (4b). (b) Calculated from extended transverse qQLCA dispersion relation (23) with Eqs. (3b), (4b), (19), and (20). The shaded region in (b) is the RPA pair excitation continuum; $\omega_0=\sqrt{2\pi ne^2/ma}$; $a=1/\sqrt{\pi n}$.

on the interlayer spacing d/a is quite pronounced, whereas its dependence on r_s is weaker (Figs. 1–3). For $d\geq a$, we calculate $C_{\pm}\approx 1.13g_{11}(r=0)+0.25+0.5\int_{0.5}^{2}dyy^{-2}g_{11}(y)$.

III. SHEAR MODE DISPERSION

We turn now to the calculation of the dispersion of the in-phase and out-of-phase shear mode oscillation frequencies based on the extended quantum QLCA [hereafter referred to as "qQLCA"] expression (13) for $\varepsilon_{\pm}^{T}(\mathbf{q},\omega)$ with the Lindhard function $\xi_0^T(\mathbf{q},\omega)$ therein given by Eq. (12). The qQLCA formalism is not geared to describing all the principal damping processes, most notably, the diffusive-migrational damping mechanism [4,5] required for the dissipation of the low-q in-phase shear mode; collisional damping is also operative, with increasing importance at higher q values. In the high-r_s Coulomb liquid phase, the latter mechanism is absent from the qQLCA model because particles on different quasi-sites are virtually isolated from each other. This leaves Landau damping (single pair excitations) as the sole mechanism responsible for the decay of collective excitations in the present study. At zero temperature, the Landau damping is confined to the RPA single-pair excitation region of the $\bar{q}$, $\bar{\omega}$–plane [shown as the shaded region in Figs. 4–10; see Appendix, Eq. (A19)]; $\bar{\omega}=\hbar\omega/\varepsilon_F$ where $\varepsilon_F=\pi n\hbar^2/m$ is the Fermi energy of the non-interacting 2D electron gas. For $\bar{\omega}\geq 0$, the equations for the left and right boundaries of the continuum are $\bar{\omega}=2\bar{q}+\bar{q}^2$ and $\bar{\omega}=-2\bar{q}+\bar{q}^2$, respectively.

The shear mode dispersion is to be calculated in the two regions of the $\bar{q},\bar{\omega}$-plane exterior to be the RPA pair excitation continuum where the modes are immune to Landau damping. From Eqs. (A24), (A26), and the relation $\xi_0^T(\mathbf{q},\omega)=(q^2c^2/\omega^2)\chi_0^T(\mathbf{q},\omega)$, the formulas for the $\xi_0^T(\mathbf{q},\omega)$ functions in these two regions are given as:

$$\xi_0^T(\mathbf{q},\omega)=-\frac{m}{\pi\hbar^2}\left[\frac{1}{6\bar{\omega}^2\bar{q}^2}\{[(\bar{\omega}-\bar{q}^2)^2-4\bar{q}^2]^{3/2}-[(\bar{\omega}+\bar{q}^2)^2-4\bar{q}^2]^{3/2}\}\right]-\frac{m}{\pi\hbar^2}\left[1+\frac{\bar{q}^4}{3\bar{\omega}^2}\right]\quad(\bar{\omega}\geq 2\bar{q}+\bar{q}^2),\tag{19}$$

$$\xi_0^T(\mathbf{q},\omega)=+\frac{m}{\pi\hbar^2}\left[\frac{1}{6\bar{\omega}^2\bar{q}^2}\{[(\bar{\omega}-\bar{q}^2)^2-4\bar{q}^2]^{3/2}+[(\bar{\omega}+\bar{q}^2)^2-4\bar{q}^2]^{3/2}\}\right]-\frac{m}{\pi\hbar^2}\left[1+\frac{\bar{q}^4}{3\bar{\omega}^2}\right]\quad(\bar{\omega}\leq -2\bar{q}+\bar{q}^2).\tag{20}$$

The starting point for the calculation of the collective mode frequencies $\omega_{\pm}(\mathbf{q})$ is the general bilayer transverse dispersion relation

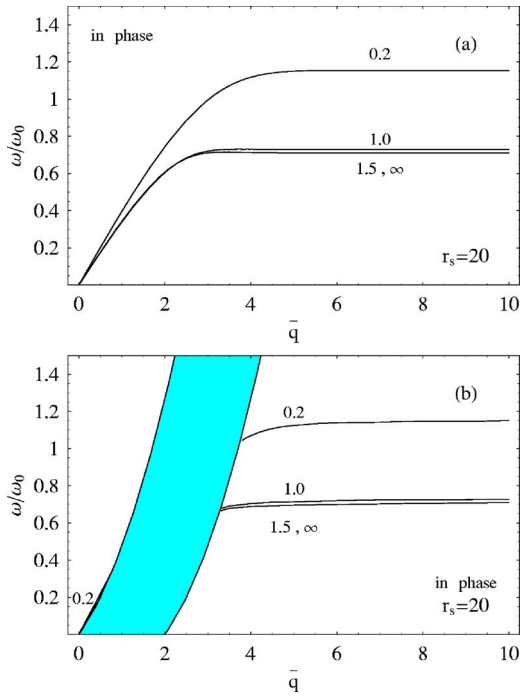

FIG. 6. (Color online) In-phase shear mode dispersion curves for $r_s=20$ and $d/a=0.2$ (normal fluid), 1.0 (normal fluid), 1.5 (fully spin-polarized fluid), and ∞ (normal fluid). (a) Calculated from primitive transverse QLCA dispersion relation (24) with Eqs. (3b) and (4b). (b) Calculated from extended transverse qQLCA dispersion relation (23) with Eqs. (3b), (4b), (19), and (20). The shaded region in (b) is the RPA pair excitation continuum; $\omega_0=\sqrt{2\pi ne^2/ma}$; $a=1/\sqrt{\pi n}$.

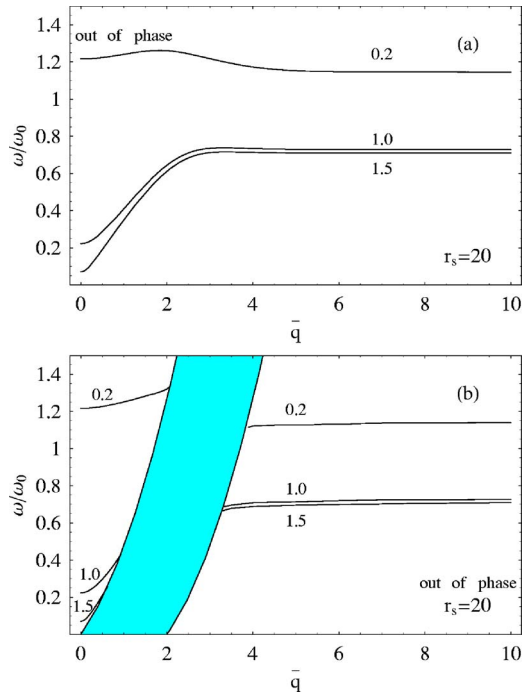

FIG. 7. (Color online) Out-of-phase shear mode dispersion curves for $r_s=20$ and $d/a=0.2$ (normal fluid), 1.0 (normal fluid), and 1.5 (fully spin-polarized fluid). (a) Calculated from primitive transverse QLCA dispersion relation (24) with Eqs. (3b) and (4b). (b) Calculated from extended transverse qQLCA dispersion relation (23) with Eqs. (3b), (4b), (19), and (20). The shaded region in (b) is the RPA pair excitation continuum; $\omega_0=\sqrt{2\pi ne^2/ma}$; $a=1/\sqrt{\pi n}$.

$$\epsilon_{\pm}^{T}(\mathbf{q},\omega)=\frac{q^2c^2}{\omega^2}. \tag{21}$$

At this stage of the development, we invoke the quasistatic approximation [5,7,9], which amounts to neglecting retardation effects by formally setting c equal to infinity. This approximation, also invoked in the derivation of Eq. (13), is tantamount to restricting our study to the (exceedingly broad) wave number domain $\bar{q}\gg\sqrt{2}r_s\epsilon_F/mc^2$. The transverse ± oscillation frequencies, $\omega_{\pm}(\mathbf{q})$, are then to be calculated from the dispersion relations

$$\frac{1}{\epsilon_{\pm}^{T}(\mathbf{q},\omega)}=0, \tag{22}$$

where from Eq. (13)

$$1+\frac{2\pi e^2}{q}\xi_0^T(\mathbf{q},\omega_{\pm}(\mathbf{q}))[G_{11}(\mathbf{q})\pm G_{12}(\mathbf{q})]=0. \tag{23}$$

In the analysis that follows, it will be of interest to compare Eq. (23) with its primitive QLCA counterpart

$$1-\frac{2\pi e^2nq}{m\omega_{\pm}^2(\mathbf{q})}[G_{11}(\mathbf{q})\pm G_{12}(\mathbf{q})]=0 \tag{24}$$

that results from Eq. (22) with the input of Eq. (2) in the quasistatic limit (nonretarded) limit. Clearly, Eq. (24) is mathematically more tractable than Eq. (23) in that (24) can be solved explicitly for $\omega_{\pm}(\mathbf{q})$ whereas (23) has to be solved numerically. However, this advantage comes at too high a cost since, for one thing, Eq. (24) does not take account of Landau damping.

We have solved both Eq. (23) [with (19) and (20)] and Eq. (24) over a wide range of r_s and d/a values, with the input of the DMC pair distribution function data generated by Rapisarda and Senatore [20,22]. The resulting dispersion curves in the $\bar{q},\bar{\omega}$-plane are displayed in Figs. 4–10. Each figure shows two panels labeled "(a)" and "(b)": the (a) panels show the dispersion curves (devoid of the RPA pair continuum) resulting from primitive QLCA Eq. (24); the (b) panels show the dispersion curves resulting from qQLCA Eq. (23). The latter, of course, are the ones that are primarily of interest in the present work. The primitive QLCA dispersion curves are displayed because it is of interest to compare them with the primitive QLCA dispersion curves in Refs. [8,9] generated from classical hypernetted-chain (HNC) radial distribution function data [30]. Two perspectives are presented: (i) In Figs. 4–8, the oscillation frequencies are normalized with respect to the nominal 2D plasma frequency $\omega_0=\sqrt{2\pi ne^2/ma}$ [the value of the 2D electron plasma frequency $\omega_{2D}(q)=\sqrt{2\pi ne^2q/m}$ at in-plane wave number $q=1/a$], and the dispersion curves are displayed as functions of d/a for fixed r_s. (ii) In Figs. 9 and 10, the oscillation frequencies are normalized with respect to the 2D Fermi frequency $\omega_F=\epsilon_F/\hbar=\pi n\hbar/m$, and the dispersion curves are displayed as functions of r_s for $d/a=0.2$.

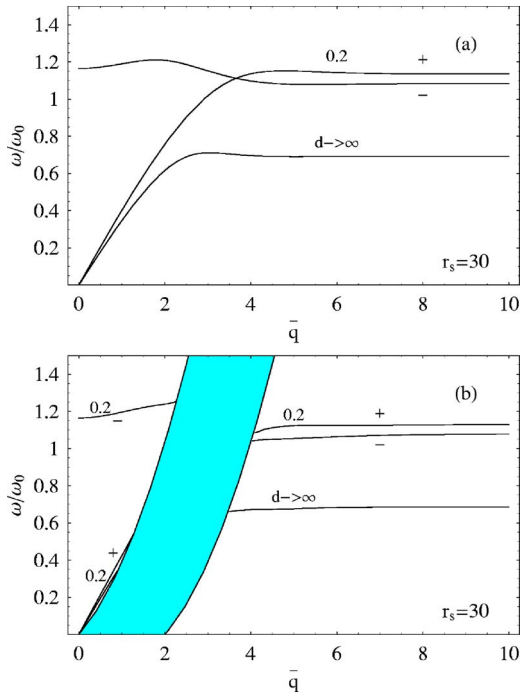

FIG. 8. (Color online) In-phase and out-of-phase dispersion curves for $r_s=30$ and $d/a=0.2$ (normal fluid) and ∞ (normal fluid). (a) Calculated from primitive transverse QLCA dispersion relation (24) with Eqs. (3b) and (4b). (b) Calculated from extended transverse qQLCA dispersion relation (23) with Eqs. (3b), (4b), (19), and (20). The shaded region in (b) is the RPA pair excitation continuum; $\omega_0=\sqrt{2\pi ne^2/ma}$; $a=1/\sqrt{\pi n}$.

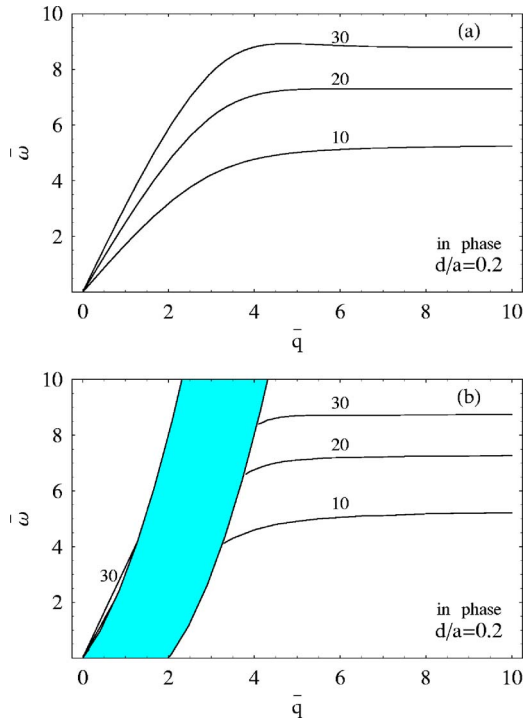

FIG. 9. (Color online) In-phase dispersion curves for $d/a=0.2$ (normal fluid) and $r_s=10,20$ and 30. (a) Calculated from primitive transverse QLCA dispersion relation (24) with Eqs. (3b) and (4b). (b) Calculated from extended transverse qQLCA dispersion relation (23) with Eqs. (3b), (4b), (19), and (20). The shaded region in (b) is the RPA pair excitation continuum; $\bar{\omega}=\hbar\omega/\epsilon_F$, $\epsilon_F=\pi n\hbar^2/m$ is the 2D Fermi energy.

We note the marked contrast between the $r_s=20$ primitive QLCA ± shear mode dispersion curves [Figs. 6(a) and 7(a)] generated from the quantum DMC $g_{AB}(r)$ data [18,20] and the corresponding $\Gamma=40$ primitive QLCA dispersion curves in Refs. [8,9] generated from classical hypernetted-chain (HNC) $g_{AB}(r)$ data [30]: The DMC-generated dispersion curves exhibit near-monotonic or only very mild oscillatory behavior, whereas the HNC-generated dispersion curves exhibit somewhat more pronounced oscillations. This difference mirrors the same dissimilar behaviors of the quantum [20,22] and classical [30] pair distribution function inputs, respectively [20]. Implicit in these dissimilar behaviors is the interplay of degeneracy, exchange, and genuine Coulomb correlation effects.

Outside the RPA single-pair excitation region, the trajectories of the out-of-phase primitive QLCA and qQLCA dispersion curves, at first glance, do not appear to be all that different from each other [Figs. 5, 7, 8, and 10]. At small layer separations, however, one difference is especially apparent: In the region above the left boundary of the RPA pair continuum the out-of-phase primitive QLCA dispersion curve [Fig. 10(a)], similarly to its classical QLCA/HNC counterpart [8,9], is concave up ($\partial^2\bar{\omega}/\partial\bar{q}^2>0$) at $\bar{q}=0$, develops an inflection point thereafter, and subsequently becomes concave down ($\partial^2\bar{\omega}/\partial\bar{q}^2<0$). By contrast, the out-of-phase qQLCA dispersion curve [Fig. 10(b)] is always concave up in the region above the RPA pair continuum and remains so right up to the continuum boundary.

At $d/a=1.5$, the separated layers become practically uncorrelated and the in-phase shear mode dispersion becomes virtually the same as the shear mode dispersion in the isolated 2D electron layer (see Figs. 4 and 6).

In the $\bar{q}=0$ limit, $\omega_+(0)=0$ and

$$\frac{\omega_-(0)}{\omega_0}=\frac{\omega_{GAP}}{\omega_0}=\sqrt{\frac{a}{2}\int_0^\infty dr\frac{rh_{12}(r)}{(r^2+d^2)^{3/2}}\left[1-\frac{3d^2}{r^2+d^2}\right]}. \tag{25}$$

The correlation-induced finite-frequency energy-gap expression (25) is formally identical to the expression for the energy gap reported in the Refs. [8,9,20] primitive QLCA [8,9] and extended qQLCA [20] studies of the out-of-phase longitudinal plasmon in charged-particle bilayer liquids. The $q=0$ gap frequency, calculated in Ref. [20] from Eq. (19) with the input of the Rapisarda-Senatore DMC data [20,22] for $h_{12}(r)$, is already displayed in Fig. 11 of Ref. [20] as a function of d/a for r_s values of 10 and 20. With increasing d/a and consequently decreasing interlayer correlations, $\omega_-(0)$ shows a decreasing tendency and it virtually vanishes for $d/a>1.5$. The $q=0$ energy gap is a unique feature of the primitive QLCA and qQLCA approaches and its existence in classical bilayers has been confirmed by recent MD simulations [10,31]. Since the physical conditions leading to the gap are similar in the classical and quantum domains, there is

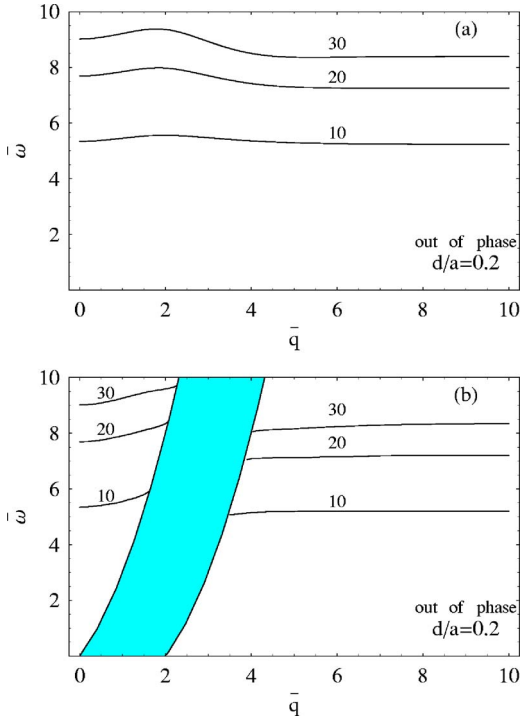

FIG. 10. (Color online) Out-of-phase dispersion curves for $d/a=0.2$ (normal fluid) and $r_s=10$, 20 and 30. (a) Calculated from primitive transverse QLCA dispersion relation (24) with Eqs. (3b) and (4b). (b) Calculated from extended transverse qQLCA dispersion relation (23) with Eqs. (3b), (4b), (19), and (20). The shaded region in (b) is the RPA pair excitation continuum; $\bar{\omega}=\hbar\omega/\epsilon_F$ where $\epsilon_F=\pi n\hbar^2/m$ is the 2D Fermi energy.

little doubt that the results of the classical MD simulations should be relevant to the Ref. [20] study and to the present work as well. Moreover, the sum-rule analysis of Ref.[32] provides a rigorous theoretical basis for expecting that the existence, but not the magnitude, of the energy gap in bilayer liquids is a statistics-independent phenomenon. We note, however, that at small layer separations, the MD gap value is about 30–40 % higher than the classical QLCA value [10]. The resolution of this discrepancy is being worked out and will be published in a future paper [33] that deals with this same issue in the broader context of asymmetric classical bilayer liquids [34] as well.

At long wavelengths, the in-phase and out-of-phase shear mode frequencies

$$\bar{\omega}_+(q\to 0)=\frac{4r_s\alpha}{\sqrt{4r_s\alpha-1}}\bar{q}, \tag{26}$$

$$\bar{\omega}_-(q\to 0)=\bar{\omega}_{GAP}+\frac{\bar{q}^2}{2\bar{\omega}_{GAP}}(1+\beta), \tag{27}$$

$$\alpha(r_s,d/a)=-\frac{1}{16}\frac{E_{11}+E_{12}}{(e^2/a)}-\frac{n}{16(e^2/a)}\frac{1}{\Omega}\times\sum_{\mathbf{q}'}\phi_{12}(q')h_{12}(q')[q'd-2q'^2d^2], \tag{28}$$

$$\beta(r_s,d/a)=-\frac{r_s}{2}\frac{E_{11}-E_{12}}{(e^2/a)}+\frac{r_s}{2}\frac{n}{(e^2/a)}\frac{1}{\Omega}\times\sum_{\mathbf{q}'}\phi_{12}(q')h_{12}(q')[q'd-2q'^2d^2], \tag{29}$$

result from the small-q expansions of Eqs. (23) and (19), using Eqs. (14) and (15); α and β are positive coefficients. Recasting (26) in the form $\bar{\omega}_+=\gamma\bar{q}$ to facilitate discussion, it is clear that for a given d/a value, there is a critical r_s value, below which $\gamma<2$, indicating a merging of the in-phase acoustic shear mode with the RPA pair continuum. To have a rough estimate of that critical value, it suffices here to consider the isolated 2D layer ($d/a\to\infty$) limit, where there is only the inlayer interaction energy, $\epsilon_{\rm int}=\epsilon_{ex}+\epsilon_{pot}$ [see Eq. (18)]; ϵ_{pot} can be readily calculated with the input of the correlation energy and its first derivative using the Tanatar-Ceperley [29] fitted MC formula (14). Our calculations indicate that γ increases from 2.035 to 2.97 as r_s increases from 10 to 30. Evidently, in the isolated 2D layer limit, the qQLCA predicts that for $r_s<10$, no transverse shear mode can propagate in the domain above the left continuum boundary. It is again instructive to note that, except for the presence of the RPA pair continuum in the zero-temperature quantum domain, the acoustic dispersion itself for the in-phase shear mode is only slightly modified by degeneracy effects in the strong coupling regime. To further demonstrate this, it suffices here to again consider the isolated 2D layer limit and compare our qQLCA shear mode acoustic dispersion coefficients ($\propto$ phase velocities) for the zero-temperature quantum liquid at $r_s=20$ and 30 with the dispersion coefficients for the finite-temperature classical liquid [5] at $\Gamma=40$ and 60, respectively (keeping in mind the correspondence $\Gamma\Leftrightarrow 2r_s$). From Eq. (26), we calculate $\omega_+(q\to 0|_{r_s=20}=0.281qa\omega_0$ and $\omega_+(q\to 0)|_{r_s=30}=0.271qa\omega_0$; these values are very nearly the same as their respective Ref. [5] finite-temperature counterparts $\omega_+(q\to 0|_{\Gamma=40}=0.279qa\omega_0$ and $\omega_+(q\to 0|_{\Gamma=60}=0.274qa\omega_0$.

Keeping this observation in mind, and the additional observation that in the classical regime, the acoustic dispersion is only very weakly dependent on coupling strength for $\Gamma>40$ (note that $\omega_+(q\to 0)=0.268qa\omega_0$ at $\Gamma=120$ [5]), we can compare the qQLCA acoustic shear mode dispersion results for the 2D zero-temperature quantum liquid with the Ref. [17] experimental measurements of transverse shear mode dispersion in 2D dusty plasma liquids. To the best of our knowledge, these measurements are the only such available on this topic in 2D and/or layered charged-particle systems. For the comparison, we select the measurements that are based on the SFACW (spatial Fourier analysis of complex wave numbers) method. Figure 11(a) shows the (solid) qQLCA acoustic dispersion curve at $r_s=20$ matched with the six SFACW-based shear mode data points at $\Gamma_x=128$, $\Gamma_y=158$; in Fig. 11(b), the qQLCA dispersion curve at $r_s=30$ is matched with the SFACW-based data near the melting point ($\Gamma\approx 200$) of the 2D dust crystal. The vertical lines on the solid theory curves mark the qa values where the acoustic lines make contact with the RPA pair continuum boundary [$qa=0.778$ for $r_s=20$ and $qa=1.344$ for $r_s=30$]. The reliabil-

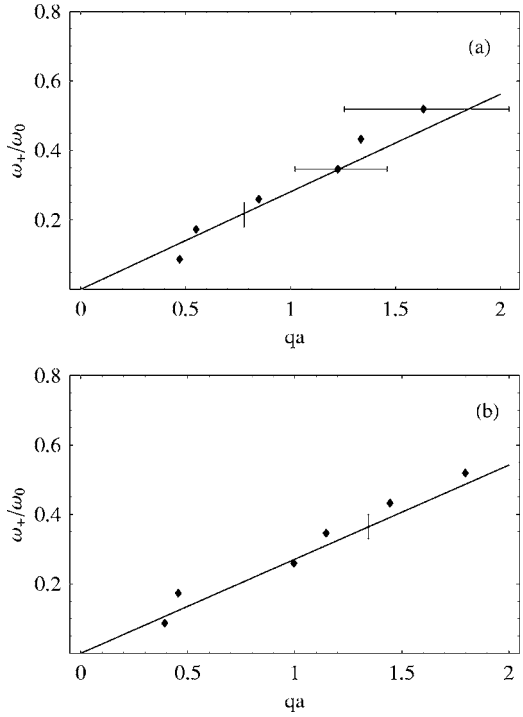

FIG. 11. In-phase shear mode dispersion for the isolated ($d/a \to \infty$) 2D charged-particle layer. Comparison of theoretical (solid lines) 2D acoustic dispersion in the zero-temperature 2D electron liquid [calculated from qQLCA Eq. (23)] with Ref. [17] SFACW experimental measurements (spatial Fourier analysis of complex wave numbers method) of shear wave dispersion in liquid 2D dusty plasma: (a) $r_s=20$ qQLCA theory matched with $\Gamma_x=128$, $\Gamma_y=158$ data (including the two horizontal error bars from Ref. [17] Fig. 8(a)); (b) $r_s=30$ qQLCA theory matched with $\Gamma \approx 200$ data. The vertical lines on the solid (theory) curves mark the qa values where the acoustic lines penetrate the RPA pair continuum boundary [$qa=0.778$ for $r_s=20$ and $qa=1.344$ for $r_s=30$].

ity of our theoretical calculations is best assessed by comparing with a sufficient number of experimental data points. To this end, to facilitate the comparison at both $r_s=20$ and 30, we can for the moment ignore the presence of the RPA pair continuum [precisely akin to the Eq. (24) primitive QLCA description] and allow the qQLCA acoustic dispersion curve to continue beyond the left boundary marker up to the qa value marking the location of the sixth data point from Ref. [17]. Agreement between theory and experiment is favorable at both r_s values.

The $r_s=10$ lower bound imposed by Landau damping notwithstanding, there is yet another damping mechanism—diffusive-migrational damping [4,5,8,9]—which is operative mostly in the region of the $\bar{q},\bar{\omega}$-plane on and above the left boundary of the RPA single-pair excitation continuum. This low-q damping mechanism will act to suppress those shear modes when their oscillation frequencies $\omega_{\pm}(\mathbf{q})$ fall below some critical frequency $\omega_{\min}=1/\tau_D$. We note, however, that the present qQLCA formalism, with its frequency-independent $G_{AB}^{T}(\mathbf{q})$, is tantamount to a static mean field theory, and, as such, is incapable of producing diffusive-migrational damping. Nevertheless, an order-of-magnitude estimate for $\omega_{\min}$ can be made based on the assumption that the shear mode disappears when the diffusion time τ_D is shorter than the oscillation period, i.e., when $\omega\tau_D \leq 1$; τ_D can be estimated as $\tau_D \approx \lambda^2/D$, where $D=\omega_0 a^2 D^*$ is the self-diffusion coefficient and λ is a characteristic migration distance of a particle from its quasisite position sufficient to disrupt the generation of the restoring shear force. Some time ago, Lee and Hong [35] and Holas, Nagano, and Singwi [36] calculated a companion transport coefficient, the intrinsic conductivity (relating to the presence of a random current), in the zero-temperature 2D electron gas free of impurities (2DEG). These inherently weak-coupling calculations of the intrinsic conductivity could shed some light on how one might proceed in the future to the calculation of the velocity autocorrelation function and self-diffusion coefficient in 2DEGs. As to the strong coupling regime, information pertaining to the self-diffusion coefficient in 2D and 3D electron liquids in the zero-temperature quantum domain is, to the best of our knowledge, lacking in the literature. Nevertheless, for the high-r_s values considered in the present work—presumably sufficient to ensure quasilocalization of the particles—one expects that self-diffusion in the strong coupling regime of the zero-temperature quantum domain should be reasonably well described by self-diffusion in the classical domain where MD data are readily available for the pure OCP in three [1,37] and two dimensions [38,39] and for the charged-particle bilayer [40]. Proceeding then on that premise, our estimates will be based on information about D extracted from the classical OCP molecular dynamics literature, keeping in mind the equivalence $\Gamma \Leftrightarrow 2r_s$ in 2D [$\Gamma=e^2/(ak_BT)$]. In the bilayer, one would expect that, as long as the liquid phase is maintained as the separation between the layers is varied [40], the self-diffusion coefficient should increase with increasing d/a reaching a maximum value at $d/a \to \infty$. Consequently, calculations of $\omega_{\min}$ based on the self-diffusion coefficients for an isolated 2D electron layer may well give overestimates of the diffusive-migrational damping $\omega_{\min}$ values for the bilayer. As in previous estimates [5,8,9], it suffices here to adapt the 3D molecular dynamics fitting formula $D^*=2.95/\Gamma^{1.34}$ [1,37] to the calculation of the 2D self-diffusion coefficient over the range of coupling values from $r_s=10$ to 30. We obtain $D(r_s=10)=0.06\omega_0 a^2$, $D(r_s=20)=0.032\omega_o a^2$, and $D(r_s=30)=0.014\omega_0 a^2$. Note how favorably the $D(r_s=20)=0.032\omega_o a^2$ value compares with the near-corresponding $D(\Gamma=36)=0.0332\omega_o a^2$ value extracted from the Ref. [38] MD simulations of the 2D OCP. Taking $\lambda=0.6a$ (note: the Lindeman melting criterion for the 2D quantum triangular crystal requires only $\lambda=0.57a$ [41]), one obtains $\omega_{\min}(r_s=10)=0.167\omega_0$, $\omega_{\min}(r_s=20)=0.089\omega_0$, and $\omega_{\min}(r_s=30)=0.039\omega_0$.

Consequently, our findings in the domain above and on the left boundary of the RPA single-pair excitation region can be summarized as follows: (i) Over the coupling range $10 \leq r_s \leq 30$, the out-of-phase gapped shear mode [Figs. 5(b), 7(b), 8(b), and 10(b)] can be safely considered not to be seriously affected by diffusive-migrational damping for $d/a \leq 0.5$. (ii) At $r_s=20$, those portions of the surviving out-of-phase dispersion curves lying above the $\omega_{\min}(r_s=20)=0.089\omega_0$ threshold will begin their trajectories as heavily damped modes for $d/a \geq 1.0$; the damping abates somewhat

with increasing q up to the left continuum boundary. (iii) At $r_s=10$, the in-phase mode [Fig. 4(b)] is suppressed by diffusive-migrational damping for all $d/a \geq 0.2$. (iv) At $r_s=20$ [Figs. 6(b) and 9(b)], the surviving portions of the in-phase acoustic dispersion curves lying above the $\omega_{\min}(r_s=20)=0.089\omega_0$ threshold are expected to be strongly to moderately damped for $d/a \geq 0.2$; the decrease in the damping with increasing wave number (for q values all the way up to the continuum boundary) is consistent with the Ref. [17] experimental findings pertaining to the damping of shear waves in liquid 2D dusty plasma. (v) At $r_s=30$ and $d/a=0.2$, where the bilayer is in a borderline normal liquid/square lattice phase, there is a substantial portion of the in-phase acoustic curve [Figs. 8(b) and 9(b)] lying above the $\omega_{\min}$ threshold that can be safely considered not to be seriously affected by diffusive-migrational damping. However, for $d/a \to \infty$ and at this r_s value, the bilayer is in the liquid phase and the surviving portion of the in-phase acoustic mode is expected to be heavily to moderately damped for q values extending all the way up to the RPA pair continuum boundary. Again, this is consistent with the Ref. [17] experimental findings cited in (iv) above.

The emergence of the qQLCA ± transverse shear mode dispersion curves from the right boundary of the single-pair excitation region [Figs. 4(b), 5(b), 6(b), 7(b), 8(b), 9(b), and 10(b)] is, to the best of our knowledge, reported here for the first time [42], though this is probably only of academic interest, since it is unlikely that these high-q modes can ultimately survive the damping mechanism due to decay into multiple pair excitations. In a highly correlated Coulomb liquid, multiple pair excitations, which are not taken into account in the present theory, are operative with increasing importance at shorter wavelengths. It is expected that the high-q portions of the emergent shear mode dispersion curve will ultimately be suppressed by this process. (This same outcome was also conjectured for the $\Gamma=40$ (corresponding to $r_s=20$) emergent dispersion curves in the classical bilayer liquid [8,9].) However, for $r_s=30$, $d/a=0.2$, where the particles are highly localized in a borderline liquid/square lattice phase [22(a),22(d)], one would expect that the ± emergent modes are immune to this process.

IV. CONCLUSIONS

In this paper, we have formulated a transverse dielectric matrix that contains information about shear mode behavior in strongly coupled symmetric charged-particle bilayer liquids in the zero-temperature quantum domain. This has been carried out over a wide range of liquid-phase coupling values $10 \leq r_s \leq 30$ and layer spacings $0.2a \leq d < \infty$. Our derivation is based on an extension of the classical quasilocalized charge approximation (QLCA) [9,16] into the quantum domain. The development of the extended transverse QLCA formalism of the present work parallels and complements the development of its Ref. [20] companion longitudinal dielectric matrix formalism.

The extended transverse QLCA formalism of the present work, referred to in the main body of the text as the qQLCA, like its Ref. [20] longitudinal counterpart, requires the input of intralayer and interlayer pair distribution function data. These were generated from diffusion Monte Carlo simulations by Rapisarda and Senatore [22] and are also displayed in Figs. 1-3 of Ref. [20].

The formulation of the transverse dielectric matrix results in the expression Eq. (13) for the in-phase (+) and out-of-phase (−) transverse dielectric functions $\epsilon_+^T(\mathbf{q},\omega)$ and $\epsilon_-^T(\mathbf{q},\omega)$, respectively, leading to a description of the two transverse collective modes via the nonretarded dispersion relation [23].

Referring to the domain of the $\bar{q},\bar{\omega}$-plane above the left boundary of the single-pair excitation region, our findings can be summarized as follows: (i) The out-of-phase gapped shear mode is robust over the Coulomb liquid-phase range $10 \leq r_s \leq 30$ for $0.2 \leq d/a \leq 0.5$; under these in-layer coupling and interlayer spacing conditions, the out-of-phase collective excitation is entirely immune to Landau damping and can be safely considered not to be seriously affected by diffusive-migrational damping. This is the main result of the present work. (ii) At $r_s=20$, those portions of the surviving out-of-phase dispersion curves lying above the $\omega_{\min}(r_s=20)=0.089\omega_0$ threshold will begin their trajectories as heavily damped modes for $d/a \geq 1.0$; the damping abates somewhat with increasing q up to the left continuum boundary. (iii) At $r_s=10$, the in-phase mode [Fig. 4(b)] is suppressed by diffusive-migrational damping for all $d/a \geq 0.2$. (iv) At $r_s=20$ [Figs. 6(b) and 9(b)], the surviving portions of the in-phase acoustic dispersion curves lying above the $\omega_{\min}(r_s=20)=0.089\omega_0$ threshold are expected to be strongly to moderately damped for $d/a \geq 0.2$; again, the damping decreases with increasing wave number up to the left boundary of the pair continuum. (v) At $r_s=30$ and $d/a=0.2$, where the bilayer is in a borderline normal liquid/square lattice phase, there is a substantial portion of the in-phase acoustic curve [Figs. 8(b) and 9(b)] lying above the $\omega_{\min}$ threshold that can be safely considered to be mostly unaffected by diffusive-migrational damping.

With the possible exception of the ($r_s=30$, $d/a=0.2$) borderline liquid/square lattice phase, the in-phase and out-of-phase shear mode dispersion curves emerging from the right boundary of the RPA single-pair excitation region are expected to be heavily damped by binary collisions. This same outcome was predicted for the emergent curves in the classical bilayer liquid [8,9] at $\Gamma=40$ (corresponding to $r_s=20$).

Note added. Further analysis of dispersion relation (23) suggests that the $r_s=20$, 30 dispersion curves [Figs. 6(b)–10(b)], in fact, can cross the left and right boundaries of the RPA single-particle excitation region and extend partially into the region. Then moving along a $\bar{\omega}(\mathbf{q};r_s)$ dispersion curve from either boundary towards the interior of the continuum, our analysis suggests that the Landau damping progressively increases from very weak [in the vicinity of the boundary where $\mathrm{Im}\xi_0^T(\mathbf{q},\omega(\mathbf{q})) \ll |\mathrm{Re}\xi_0^T(\mathbf{q},\omega(\mathbf{q}))|$] to strong, intensifying to the point where the mode becomes too heavily damped to survive. For example, at $r_s=20$ and $d/a=0.2$, the out-of-phase mode enters the left boundary at $\bar{q}_L=2.07$ and persists somewhat beyond $\bar{q}=2.3$ where the Landau damping rate has reached a value $|\bar{\gamma}_L| \sim 0.11\bar{\omega}$. The mode then ceases to be viable within the open interval 2.3

$<\bar{q}<3.2$. The $\bar{q}=3.2$ upper bound marks the point where $|\bar{\gamma}_L|\sim 0.14\bar{\omega}$, and where the mode can thus be considered to be revived, becoming more and more robust as $\bar{q}$ increases beyond 3.2; the dispersion curve subsequently emerges from the right boundary at $\bar{q}_R=3.84$ entirely free of Landau damping.

ACKNOWLEDGMENTS

This material was based upon work supported by the National Science Foundation under Grant Nos. PHY-0206554 and PHY-0514618. K.I.G. thanks Gabor Kalman and M. Howard Lee for helpful discussions.

APPENDIX

In this Appendix, we present a derivation of the Lindhard transverse (T) dielectric function, $\epsilon_0^T(\mathbf{q},\omega)$, for the two-dimensional free-electron gas; external magnetic fields are assumed to be entirely absent. The derivation parallels the Ehrenreich-Cohen [24] and Kliewer-Fuchs [25] self-consistent field (SCF) calculations for the three-dimensional electron gas. We explicitly evaluate $\epsilon_0^T(\mathbf{q},\omega)$ at zero temperature both inside and outside the RPA single-particle excitation region of the ω,q-plane. The Coulomb gauge is assumed throughout.

Let the 2DEG occupy the $z=0$ plane of a Cartesian coordinate system and let $\mathbf{A}(\mathbf{x},t)$ be the *total* self-consistent vector potential response to a small electromagnetic disturbance. The resulting single-particle Hamiltonian for an electron having charge $-e$ and mass m is

$$H=\frac{1}{2m}\left[\mathbf{p}+\frac{e}{c}\mathbf{A}\right]^2+\Phi; \tag{A1}$$

$\mathbf{p}$ is the canonical momentum. Carrying out the routine linear response calculation, let $H=H_0+H_1$, where the stationary states of the free-electron Hamiltonian, $H_0=p^2/2m$, are characterized by the wave functions $|\mathbf{k}\rangle\leftrightarrow\sqrt{1/\Omega}\exp(i\mathbf{k}\cdot\mathbf{x})$ and their corresponding eigenvalues $\epsilon_\mathbf{k}=\hbar^2k^2/2m$, viz.

$$H_0|\mathbf{k}\rangle=\epsilon_\mathbf{k}|\mathbf{k}\rangle. \tag{A2}$$

To lowest order in $\mathbf{A}$

$$H_1=\frac{e}{2mc}(\mathbf{p}\cdot\mathbf{A}+\mathbf{A}\cdot\mathbf{p})+\Phi. \tag{A3}$$

Accordingly, the linearized equation of motion for the single-particle density matrix ρ is

$$i\hbar\frac{\partial\rho}{\partial t}=[H_0,\rho_1]+[H_1\rho_0]; \tag{A4}$$

$\rho=\rho_0+\rho_1$, ρ_1 being the perturbed part of ρ associated with H_1. In virtue of (A2), the unperturbed density matrix operator $\rho_0=f(H_0)$ has the property that $\rho_0|\mathbf{k}\rangle=f(\epsilon_\mathbf{k})|\mathbf{k}\rangle$, where $f(\epsilon_\mathbf{k})=\{1+\exp[(\epsilon_\mathbf{k}-\mu)/kT]\}^{-1}$ is the equilibrium Fermi function for a free electron with energy $\epsilon_\mathbf{k}$. Taking matrix elements of (A4) between states $|\mathbf{k}\rangle$ and $|\mathbf{k}+\mathbf{q}\rangle$ and Fourier transforming to the frequency domain, one obtains

$$\langle\mathbf{k}|\rho_1(\omega)|\mathbf{k}+\mathbf{q}\rangle=\frac{f(\epsilon_{\mathbf{k}+\mathbf{q}})-f(\epsilon_\mathbf{k})}{\epsilon_{\mathbf{k}+\mathbf{q}}-\epsilon_\mathbf{k}+\hbar\,\omega}H_\mathbf{q}(\omega), \tag{A5}$$

$$H_\mathbf{q}(\omega)=\langle\mathbf{k}|H_1(\omega)|\mathbf{k}+\mathbf{q}\rangle=\frac{e\hbar}{2mc}\frac{1}{\Omega}(2\mathbf{k}+\mathbf{q})\cdot\mathbf{A}(-\mathbf{q},\omega)+\frac{1}{\Omega}\Phi(-\mathbf{q},\omega), \tag{A6}$$

$(1/\Omega)\mathbf{A}(-\mathbf{q},\omega)=\langle\mathbf{k}|\mathbf{A}(\mathbf{x},\omega)|\mathbf{k}+\mathbf{q}\rangle$. The average transverse current density response, $\mathbf{j}(\mathbf{r},\omega)$, at field point $\mathbf{r}$ is given by the trace of the product of the density matrix and the single-particle current density operator $-(e/2)[\delta(\mathbf{r}-\mathbf{x})\mathbf{v}+\mathbf{v}\delta(\mathbf{r}-\mathbf{x})]$, where the velocity operator $\mathbf{v}=(1/m)[\mathbf{p}+(e/c)\mathbf{A}]$. To linear order, the calculation then proceeds as follows:

$$\begin{aligned}\mathbf{j}(\mathbf{r},\omega)&=-\frac{e}{2m}\mathrm{Tr}\{[\mathbf{p}\delta(\mathbf{r}-\mathbf{x})+\delta(\mathbf{r}-\mathbf{x})\mathbf{p}]\rho_1(\omega)\}\\&\quad-\frac{e^2}{mc}\mathrm{Tr}\{\mathbf{A}(\mathbf{x},\omega)\delta(\mathbf{r}-\mathbf{x})\rho_0\}\\&=-\frac{e}{2m}2\sum_{\mathbf{k}'}[\langle\mathbf{k}'|\mathbf{p}\delta(\mathbf{r}-\mathbf{x})\rho_1(\omega)|\mathbf{k}'\rangle\\&\quad+\langle\mathbf{k}'|\delta(\mathbf{r}-\mathbf{x})\mathbf{p}\rho_1(\omega)|\mathbf{k}'\rangle]\\&\quad-\frac{e^2}{mc}2\sum_{\mathbf{k}'}\langle\mathbf{k}'|\mathbf{A}(\mathbf{x},\omega)\delta(\mathbf{r}-\mathbf{x})\rho_0|\mathbf{k}'\rangle\\&=-\frac{e\hbar}{m}\frac{1}{\Omega}\sum_{\mathbf{k},\mathbf{q}'}(2\mathbf{k}+\mathbf{q}')e^{-i\mathbf{q}'\cdot\mathbf{r}}\langle\mathbf{k}|\rho_1(\omega)|\mathbf{k}+\mathbf{q}'\rangle\\&\quad-\frac{ne^2}{mc}\mathbf{A}(\mathbf{r},\omega),\end{aligned} \tag{A7}$$

$n=(2\Omega)\Sigma_\mathbf{k}f(\epsilon_\mathbf{k})$ is the 2D unperturbed particle density. The "2" factor in front of the summation signs is due to the two spin states. Equations (A5) and (A6), when combined with the spatial Fourier transform of (A7), then give

$$\begin{aligned}\mathbf{j}(\mathbf{q},\omega)&=-\frac{2e^2\hbar^2}{m^2c}\left[\frac{1}{\Omega}\sum_\mathbf{k}\left[\mathbf{k}+\frac{\mathbf{q}}{2}\right]\left[\mathbf{k}+\frac{\mathbf{q}}{2}\right]\right.\\&\quad\left.\times\frac{f(\epsilon_{\mathbf{k}+\mathbf{q}})-f(\epsilon_\mathbf{k})}{\epsilon_{\mathbf{k}+\mathbf{q}}-\epsilon_\mathbf{k}+\hbar\,\omega}\right]\cdot\mathbf{A}(\mathbf{q},\omega)\\&\quad+\frac{2e\hbar}{m\Omega}\sum_\mathbf{k}\left[\mathbf{k}+\frac{\mathbf{q}}{2}\right]\frac{f(\epsilon_{\mathbf{k}+\mathbf{q}})-f(\epsilon_\mathbf{k})}{\epsilon_{\mathbf{k}+\mathbf{q}}-\epsilon_\mathbf{k}+\hbar\,\omega}\Phi(\mathbf{q},\omega)\\&\quad-\frac{ne^2}{mc}\mathbf{A}(\mathbf{q},\omega).\end{aligned} \tag{A8}$$

Without any loss of generality, we can take $\mathbf{q}=(q,0,0)$ and $\mathbf{A}=(0,A,0)$, so that the relevant transverse component of (A8) simplifies to

$$j_y(q,\omega) = -\frac{2e^2\hbar^2}{m^2c}\left[\frac{1}{\Omega}\sum_{\mathbf{k}} k_y^2 \frac{f(\epsilon_{\mathbf{k}+\mathbf{q}}) - f(\epsilon_{\mathbf{k}})}{\epsilon_{\mathbf{k}+\mathbf{q}} - \epsilon_{\mathbf{k}} + \hbar\,\omega}\right] A(q,\omega) - \frac{ne^2}{mc} A(q,\omega). \tag{A9}$$

Comparison with the 2D constitutive relation [26]

$$j_y(q,\omega) = \frac{\omega^2}{2\pi\beta(q,\omega)c}[\epsilon_0^T(q,\omega) - 1]A(q,\omega), \tag{A10}$$

then yields

$$\epsilon_0^T(q,\omega) = 1 - \frac{\omega_{2D}^2(q)}{\omega^2}\frac{\beta(q,\omega)}{q}[1 + W(\mathbf{q},\omega)], \tag{A11}$$

$$W(q,\omega) = \frac{2}{N}\sum_{\mathbf{k}} \frac{\hbar^2 k_y^2}{m} \frac{f(\epsilon_{\mathbf{k}+\mathbf{q}}) - f(\epsilon_{\mathbf{k}})}{\epsilon_{\mathbf{k}+\mathbf{q}} - \epsilon_{\mathbf{k}} + \hbar\,\omega + io}, \tag{A12}$$

$\beta(q,\omega) = \sqrt{q^2 - \omega^2/c^2}$ is the familiar attenuation constant that shows up in 2D phenomenological electrodynamics [26] and $\omega_{2D}(q) = \sqrt{2\pi ne^2 q/m}$ is the 2D RPA plasma frequency. In the finite-temperature, nonretarded classical (cl) limit, one recovers from (A11) the well-known Vlasov expression [5]

$$\epsilon_0^T(q,\omega)\Big|_{cl} = 1 - \frac{\omega_{2D}^2(q)}{n\omega}\int d^2\mathbf{v}\frac{F^{(0)}(\mathbf{v})}{\omega - \mathbf{q}\cdot\mathbf{v} + io}, \tag{A13}$$

$F^{(0)}(\mathbf{v}) = n(\beta m/2\pi)\exp(-\beta m v^2/2)$ is the Maxwellian distribution function. As an aside, we note the marked structural difference between the transverse RPA expressions (A11) and (A13) and their respective longitudinal RPA quantum [24,43,44] and classical counterparts

$$\epsilon_0^L(q,\omega) = 1 - \frac{2\pi e^2}{q}\frac{2}{A}\sum_{\mathbf{k}} \frac{f(\epsilon_{\mathbf{k}+\mathbf{q}}) - f(\epsilon_{\mathbf{k}})}{\epsilon_{\mathbf{k}+\mathbf{q}} - \epsilon_{\mathbf{k}} + \hbar\,\omega + io}, \tag{A14}$$

$$\epsilon_0^L(q,\omega)\big|_{cl} = 1 + \frac{\kappa}{q}\left[1 - \frac{\omega}{n}\int d^2\mathbf{v}\frac{F^{(0)}(\mathbf{v})}{\omega - \mathbf{q}\cdot\mathbf{v} + io}\right], \tag{A15}$$

$\kappa = 2\pi\beta ne^2$ is the 2D Debye length.

The explicit evaluation of (A11) in the zero temperature quantum domain is carried out by first recasting (A12) in the more convenient integral form

$$W(\mathbf{q},\omega) = \frac{1}{2\pi^2 n}\int d\mathbf{k}\frac{\hbar^2 k_y^2}{m} f(\mathbf{k}) \times\left[\frac{1}{\omega + \hbar\,\mathbf{k}\cdot\mathbf{q}/m - \hbar\,q^2(2m) + io} - \frac{1}{\omega + \hbar\,\mathbf{k}\cdot\mathbf{q}/m + \hbar\,q^2/(2m) + io}\right], \tag{A16}$$

which, at zero temperature, becomes

$$W(\mathbf{q},\omega) = \frac{\hbar}{\pi^2 mn}\int_{-k_F}^{k_F} dk_x (k_F^2 - k_x^2)^{3/2} \times\left[\frac{1}{\omega + \hbar\,qk_x/m - \hbar\,q^2/(2m) + io} - \frac{1}{\omega + \hbar\,qk_x/m + \hbar\,q^2/(2m) + io}\right], \tag{A17}$$

$k_F = \sqrt{2\pi n}$ is the 2D Fermi wave number. Separating the real and imaginary parts,

$$\mathrm{Re}\, W(\mathbf{q},\omega) = \frac{\hbar}{\pi^2 mn}\int_{-k_F}^{k_F} dk_x (k_F^2 - k_x^2)^{3/2} \times P\left[\frac{1}{\omega + \hbar\,qk_x/m - \hbar\,q^2/(2m)} - \frac{1}{\omega + \hbar\,qk_x/m + \hbar\,q^2/(2m)}\right], \tag{A18}$$

$$\mathrm{Im}\, W(\mathbf{q},\omega) = -\frac{1}{\pi nq}\left[k_F^2 - \left[\frac{m\omega}{\hbar q} - \frac{q}{2}\right]^2\right]^{3/2} \times\left\{\theta\left[\frac{\hbar qk_F}{m} + \frac{\hbar q^2}{2m} - \omega\right] - \theta\left[-\frac{\hbar qk_F}{m} + \frac{\hbar q^2}{2m} - \omega\right]\right\} + \frac{1}{\pi nq} \times\left[k_F^2 - \left[\frac{m\omega}{\hbar q} + \frac{q}{2}\right]^2\right]^{3/2}\theta\left[\frac{\hbar qk_F}{m} - \frac{\hbar q^2}{2m} - \omega\right], \tag{A19}$$

where θ is the unit step function. The further explicit evaluation of the Eq. (A18) expression for Re $W(\mathbf{q},\omega)$ in the regions of the q,ω-plane exterior to the RPA pair continuum is facilitated by introducing the current-density response function via the constitutive relation [26]

$$\mathbf{j}(\mathbf{q},\omega) = e^2 c\chi_T(\mathbf{q},\omega)\mathbf{A}(\mathbf{q},\omega). \tag{A20}$$

The Lindhard transverse current density response function

$$\chi_0^T(\mathbf{q},\omega) = -\frac{n}{mc^2}[1 + W(\mathbf{q},\omega)] \tag{A21}$$

then results from comparison of (A11) with

$$\epsilon_0^T(\mathbf{q},\omega) = 1 + \frac{q^2c^2}{\omega^2}\psi(q,\omega)\chi_0^T(\mathbf{q},\omega), \tag{A22}$$

where $\psi(q,\omega) = (2\pi e^2/q^2)\beta(q,\omega)$ is the 2D effective interaction potential. We next introduce the convenient dimensionless quantities $\bar{q} = q/k_F$ and $\bar{\omega} = \hbar\,\omega/\epsilon_F$; $\epsilon = \pi n\hbar^2/m$ is the 2D Fermi energy for the non-interacting electron gas at zero temperature. The following expressions result:

Above the left boundary of the pair continuum ($\bar{\omega} \geq 2\bar{q} + \bar{q}^2$),

$$\epsilon_0^T(\bar{q},\bar{\omega}) = 1 - \frac{\omega_{2d}^2(q)}{\omega^2}\frac{\beta(q,\omega)}{q}\frac{1}{12\bar{q}^4}[[(\bar{\omega}-\bar{q}^2)^2-4\bar{q}^2]^{3/2} - [(\bar{\omega}+\bar{q}^2)^2-4\bar{q}^2]^{3/2}] - \frac{\omega_{2d}^2(q)}{\omega^2}\frac{\beta(q,\omega)}{q} \times \left[\frac{\bar{\omega}^2}{2\bar{q}^2}+\frac{\bar{q}^2}{6}\right] = 1 + \frac{q^2c^2}{\omega^2}\psi(q,\omega)\chi_0^T(\mathbf{q},\omega), \tag{A23}$$

$$\chi_0^T(\mathbf{q},\omega) = -\frac{n}{mc^2}\frac{1}{12\bar{q}^4}[[(\bar{\omega}-\bar{q}^2)^2-4\bar{q}^2]^{3/2} - [(\bar{\omega}+\bar{q}^2)^2-4\bar{q}^2]^{3/2}+6\bar{\omega}^2\bar{q}^2+2\bar{q}^6]. \tag{A24}$$

Below the right boundary of the pair continuum ($0 \le \bar{\omega} \le -2\bar{q}+\bar{q}^2$),

$$\epsilon_0^T(\bar{q},\bar{\omega}) = 1 + \frac{\omega_{2d}^2(q)}{\omega^2}\frac{\beta(q,\omega)}{q}\frac{1}{12\bar{q}^4}[[(\bar{\omega}-\bar{q}^2)^2-4\bar{q}^2]^{3/2} + [(\bar{\omega}+\bar{q}^2)^2-4\bar{q}^2]^{3/2}] - \frac{\omega_{2d}^2(q)}{\omega^2}\frac{\beta(q,\omega)}{q} \times \left[\frac{\bar{\omega}^2}{2\bar{q}^2}+\frac{\bar{q}^2}{6}\right], \tag{A25}$$

$$\chi_0^T(\bar{q},\bar{\omega}) = +\frac{n}{mc^2}\frac{1}{12\bar{q}^4}[[(\bar{\omega}-\bar{q}^2)^2-4\bar{q}^2]^{3/2} + [(\bar{\omega}+\bar{q}^2)^2-4\bar{q}^2]^{3/2}-6\bar{\omega}^2\bar{q}^2-2\bar{q}^6]. \tag{A26}$$

[1] J.-P. Hansen, I. R. McDonald, and E. L. Pollock, Phys. Rev. A **11**, 1025 (1975).
[2] H. Totsuji and H. Kakeya, Phys. Rev. A **22**, 1220 (1980).
[3] G. K. Agarwal, J. S. Thakur, and K. N. Pathak, Phys. Lett. **84A**, 213 (1981); G. K. Agarwal and K. N. Pathak, J. Phys. C **15**, 5063 (1982).
[4] K. I. Golden, G. Kalman, and Ph. Wyns, Phys. Rev. A **46**, 3454 (1992).
[5] K. I. Golden, G. Kalman, and Ph. Wyns, Phys. Rev. A **46**, 3463 (1992).
[6] P. Schmidt, G. Zwicknagel, P.-G. Reinhard, and C. Toepffer, Phys. Rev. E **56**, 7310 (1997).
[7] K. I. Golden, G. Kalman, L. Miao, and R. R. Snapp, Phys. Rev. B **55**, 16349 (1997); **57**, 9883 (1998).
[8] G. Kalman, V. Valtchinov, and K. I. Golden, Phys. Rev. Lett. **82**, 3124 (1999); **91**, 159901(E) (2003).
[9] K. I. Golden and G. J. Kalman, Phys. Plasmas **7**, 14 (2000); **8**, 5064 (2001).
[10] Z. Donko, G. J. Kalman, P. Hartmann, K. I. Golden, and K. Kutasi, Phys. Rev. Lett. **90**, 226804 (2003); Z. Donko, P. Hartmann, G. J. Kalman, and K. I. Golden, J. Phys. A **36**, 5877 (2003).
[11] H. Ohta and S. Hamaguchi, Phys. Rev. Lett. **84**, 6026 (2000).
[12] G. Kalman, M. Rosenberg, and H. E. DeWitt, Phys. Rev. Lett. **84**, 6030 (2000).
[13] G. J. Kalman, P. Hartmann, Z. Donko, and M. Rosenberg, Phys. Rev. Lett. **92**, 065001 (2004).
[14] P. K. Kaw and A. Sen, Phys. Plasmas **5**, 3116 (1998).
[15] M. S. Murillo, Phys. Rev. Lett. **85**, 2514 (2000).
[16] G. Kalman and K. I. Golden, Phys. Rev. A **41**, 5516 (1990).
[17] A. Piel, V. N. Nosenko, and J. Goree, Phys. Plasmas **13**, 042104 (2006).
[18] S. Shapira, U. Sivan, P. M. Solomon, E. Buchstab, M. Tischler, and G. Ben Yoseph, Phys. Rev. Lett. **77**, 3181 (1996); Y. Hanein, H. Shtrikman, and U. Meirav, Appl. Phys. Lett. **70**, 1426 (1997); M. Y. Simmons, A. R. Hamilton, S. J. Stevens, D. A. Ritchie, and M. Pepper, *ibid.* **70**, 2750 (1997); Y. Hanein, H. Shtrikman, and U. Meirav, Physica E (Amsterdam) **2**, 498 (1998); H. Shtrikman, Y. Hanein, A. Soibel, and U. Meirav, Microelectron. J. **30**, 323 (1999); S. Ilani, A. Yacoby, D. Mahalu, and H. Shtrikman, Phys. Rev. Lett. **84**, 3133 (2000). Y. Y. Proskuryakov, A. K. Savchenko, S. S. Safonov, M. Pepper, M. Y. Simmons, and D. A. Ritchie, *ibid.* **86**, 4895 (2001).
[19] M. A. Eriksson, A. Pinczuk, B. S. Dennis, C. F. Hirjibeheden, S. H. Simon, L. N. Pfeiffer, and K. W. West, Physica E (Amsterdam) **6**, 165 (2000); C. F. Hirjibehedin, A. Pinczuk, B. S. Dennis, L. N. Pfeiffer, and K. W. West, Phys. Rev. B **65**, 161309(R) (2002).
[20] K. I. Golden, H. Mahassen, G. J. Kalman, G. Senatore, and F. Rapisarda, Phys. Rev. E **71**, 036401 (2005).
[21] K. I. Golden, H. Mahassen, and G. J. Kalman, Phys. Rev. E **70**, 026406 (2004).
[22] F. Rapisarda and G. Senatore, in *Strongly Coupled Coulomb Systems*, edited by G. Kalman, K. Blagoev, and M. Rommel (Plenum Press, New York, 1998), p. 529; Aust. J. Phys. **49**, 161 (1996); F. Rapisarda, Ph.D. thesis, University of Trieste, 1966; G. Senatore, F. Rapisarda, and S. Conti, Int. J. Mod. Phys. B **13**, 479 (1999); Gaetano Senatore (senatore@ts.infn.it); for a recent comprehensive study of the ground-state behavior of the symmetric electron bilayer that compares the qSTLS, STLS, and diffusion Monte Carlo approaches, see R. K. Moudgil, G. Senatore, and L. K. Saini, Phys. Rev. B **66**, 205316 (2002).
[23] T. Toyoda, V. Gudmundsson, and Takahashi, Physica A **127A**, 529 (1984); R. Nifosi, S. Conti, and M. P. Tosi, e-print cond-mat/9807085.
[24] H. Ehrenreich and M. H. Cohen, Phys. Rev. **115**, 786 (1959).
[25] K. L. Kliewer and R. Fuchs, Phys. Rev. **181**, 552 (1969).
[26] K. I. Golden and G. Kalman, Phys. Rev. B **45**, 5834 (1992).
[27] K. I. Golden and G. Kalman, Phys. Rev. B **52**, 14719 (1995).
[28] F. Lado, Phys. Rev. B **17**, 2827 (1978).
[29] B. Tanatar and D. M. Ceperley, Phys. Rev. B **39**, 5005 (1989).
[30] V. I. Valtchinov, G. Kalman, and K. B. Blagoev, Phys. Rev. E **56**, 4351 (1997); G. J. Kalman, K. B. Blagoev, Z. Donko, K. I. Golden, G. McMullan, V. Valtchinov, and H. Zhao, J. Phys. IV **10**, Pr5-85 (2000).

[31] S. Ranganathan and R. E. Johnson, Phys. Rev. B **69**, 085310 (2004).
[32] K. I. Golden and G. J. Kalman, J. Phys. A **36**, 5865 (2003).
[33] G. J. Kalman, Z. Donko, K. I. Golden, and G. Kalman (unpublished).
[34] H. Mahassen, K. Kutasi, K. I. Golden, G. J. Kalman, and Z. Donko, J. Phys. A **39**, 4601 (2006).
[35] M. H. Lee and J. Hong, Phys. Rev. Lett. **48**, 634 (1982); Phys. Rev. B **26**, 2227 (1982); Physica (Utrecht) **128B**, 301 (1985); Phys. Rev. B **32**, 7734 (1985).
[36] A. Holas, S. Nagano, and K. S. Singwi, Phys. Rev. B **27**, 5981 (1983).
[37] Z. Donko, G. J. Kalman, and K. I. Golden, Phys. Rev. Lett. **88**, 225001 (2002).
[38] J.-P. Hansen, D. Levesque, and J. J. Weis, Phys. Rev. Lett. **43**, 979 (1979).
[39] B. Singla, K. Tankeshwar, and K. N. Pathak, Phys. Rev. A **41**, 4306 (1990).
[40] S. Ranganathan, R. E. Johnson, and K. N. Pathak, Phys. Rev. E **65**, 051203 (2002).
[41] D. Ceperley, Phys. Rev. B **18**, 3126 (1978).
[42] Figures 1 and 2 of Ref. [8] also show shear (and plasmon) dispersion curves emerging from the right boundary. However, we remind the reader that the Ref. [8] QLCA treatment is strictly classical with the RPA single-pair excitation region overlaid on the dispersion curves to allow for a qualitative assessment of the effect of Landau damping on the collective modes in zero-temperature bilayer liquids.
[43] J. K. Lindhard, K. Dan. Vidensk. Selsk. Mat. Fys. Medd. **28**, No. 8 (1954).
[44] A. Bret and C. Deutsch, Phys. Rev. E **48**, 2994 (1993).